Aalborg Universitet

AALBORG UNIVERSITY

System-Level Thermal Modeling of a Modular Multilevel Converter

Zhang, Yi; Wang, Huai; Wang, Zhongxu; Blaabjerg, Frede

Published in:
2020 IEEE Applied Power Electronics Conference and Exposition (APEC)

DOI (link to publication from Publisher):
10.1109/APEC39645.2020.9124434

Publication date:
2020

Document Version
Accepted author manuscript, peer reviewed version

Link to publication from Aalborg University

Citation for published version (APA):
Zhang, Y., Wang, H., Wang, Z., & Blaabjerg, F. (2020). System-Level Thermal Modeling of a Modular Multilevel Converter. In *2020 IEEE Applied Power Electronics Conference and Exposition (APEC)* (pp. 2766-2771). Article 9124434 IEEE (Institute of Electrical and Electronics Engineers). https://doi.org/10.1109/APEC39645.2020.9124434

General rights
Copyright and moral rights for the publications made accessible in the public portal are retained by the authors and/or other copyright owners and it is a condition of accessing publications that users recognise and abide by the legal requirements associated with these rights.

- Users may download and print one copy of any publication from the public portal for the purpose of private study or research.
- You may not further distribute the material or use it for any profit-making activity or commercial gain
- You may freely distribute the URL identifying the publication in the public portal -

Take down policy
If you believe that this document breaches copyright please contact us at vbn@aub.aau.dk providing details, and we will remove access to the work immediately and investigate your claim.

Downloaded from vbn.aau.dk on: December 06, 2025

System-Level Thermal Modeling of a Modular Multilevel Converter

Yi Zhang, Huai Wang, Zhongxu Wang, and Frede Blaabjerg
Department of Energy Technology, Aalborg University, Denmark
E-mail: yiz@et.aau.dk, hwa@et.aau.dk, zho@et.aau.dk, and fbl@et.aau.dk

***Abstract*—In the thermal analysis of a Modular Multilevel Converter (MMC) system, one of the challenges is to model the heat sources and thermal paths across large spatial scales, i.e., from a tiny power semiconductor chip at square millimeters to the whole converter system up to several thousand cubic meters. Without good understanding of the dissimilarity of thermal behaviors under different spatial scales, conventional thermal models usually lead to either considerable modeling errors or heavy computational burden. In this paper, a hierarchical decomposition method is proposed to do the system-level thermal modeling of the MMC. At Sub-Module(SM) level, ethe junction/hotspot-to-local ambient thermal model of devices is established, where Thermal Cross-Coupling (TCC) effects among different devices in the SM are considered. At converter-level, thermal model is obtained to depict mutual influences among the SMs in the MMC. A 15-kVA MMC prototype provides the experimental verifications at last.**

I. Introduction

With the Modular Multilevel Converter (MMC) widely implemented in many applications [1]–[4], its reliability challenges are emerging. These challenges come from a large number of reliability-critical components in the MMC (e.g., Insulated-Gate Bipolar Transistors (IGBTs), capacitors, etc.), but also due to much harsher working conditions [5].

Temperature is one of the most significant stressors which affect the lifetime of power electronic components and systems [6]. As a result, thermal modeling is essential to the degradation analysis of these critical components and systems. For the power semiconductor devices in the MMC, many studies have discussed its thermal model [7]–[11]. The typically used thermal model is the one-dimensional (1-D) RC lumped Foster network as shown in Fig. 1(a), which is normally provided by manufacturers in datasheets [12]. The 1-D Foster network might be reasonable for discrete packaging devices. However, when it comes to the power module packaging with multi-chips, Thermal Cross-Coupling (TCC) effects occur among different chips within the same package even if different sub-systems are mounted in the same cabinet, as shown in Fig. 1 (b). The conventional 1-D Foster network neglects the TCC effect and might lead to misleading thermal estimation. The Finite-Element Method (FEM) simulation can model the TCC effect among different devices or sub-systems. However, since the MMC usually has many Sub-Modules (SMs) and a large volume, the FEM simulation of the complete system is challenging to compute the thermal paths across large spatial scales.

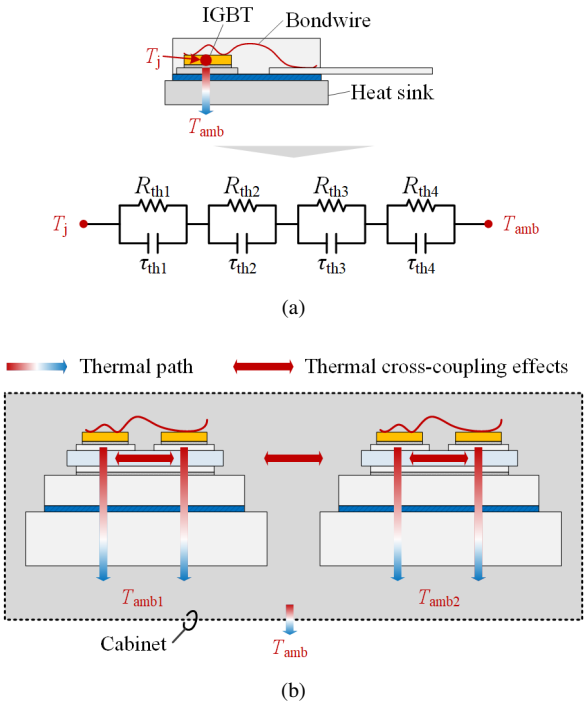

Fig. 1. Comparison between thermal networks of a discrete packaging device and a system: (a) the discrete packaging device and the 1-D Foster network and (b) a system configuration consists of the cabinet, two sub-systems, and power modules with multiple chips.

Beyond the MMC application, references [13], [14] have pointed out that the TCC effect has significant impacts on device temperatures. Existing literatures are is mostly limited to applications such as motor drives, PV inverters (volume $\leq$ 1 m^3), etc., where all the devices are assumed to be exposed to the same environmental conditions. The TCC effects among sub-systems are rarely discussed. For the MMC, both the electric rating and footprint are far beyond the scope of conventional power electronic systems. The assumption of homogeneous environmental temperatures for all the devices is questionable. Therefore, the system-level thermal investigation of the MMC is necessary to be studied.

This paper proposes a system-level thermal model for the MMC. The comprehensive TCC effects cover the thermal behaviors among devices, sub-systems, and the impact of the cabinet. Based on a 15-kVA MMC prototype, an in-situ measurement verifies the effectiveness of the proposed

method.

II. Configuration of a 15-kVA MMC Prototype

In the paper, a 15 kVA down-scale MMC prototype has been built, as shown in Fig. 2. The environmental cooling air is imported from the bottom and backside grilles of the cabinet. The hot air exhausts via the top-side fans. In the circuit configuration, each phase of the MMC comprises two arms, and each arm consists of 4 SMs and an arm inductor. In each SM, a half-bridge circuit has two IGBTs (denoted as S_1 and S_2) and two diodes (D_1 and D_2). Meanwhile, two capacitors in parallel consist of the capacitor bank. In order to measure the junction/hotspot temperatures of devices, four thermo-optical fibers are mounted on the surface of the semiconductor chips (see Fig. 3), and two K-type thermal couples are embedded inside the two capacitors. Simultaneously, the local ambient temperatures of SMs, which are defined as the environmental temperature around the SM, are monitored by 24 K-type thermal couples. In the following analysis, each inductor and SM are given a unique label as $\{\mathrm{L1}, \mathrm{L2}, ..., \mathrm{L6}, \mathrm{SM1}, \mathrm{SM2}, ..., \mathrm{SM24}\}$. The critical components of each SM $\{S_1, S_2, D_1, D_2, C_1, C_2, R_b\}$ are also allocated labels as $\{1, 2, ..., 6, \mathrm{R}\}$, respectively.

III. Systematica Thermal Model of the MMC

The establishment or characterization of a thermal model usually needs the assist of measurements or Finite-Element-Method (FEM) simulations. However, for the MMC system with hundreds or thousands of SMs in practice, it is challenging to measure or simulate the complete MMC system. In this section, a hierarchical decomposition method is proposed for the system-level thermal modeling of the MMC, namely the SM and converter levels. In the first thermal modeling (SM-level), the junction/hotspot-to-local ambient thermal model of each device is established. The TCC effect considers the mutual influences among devices. Moreover, in the second thermal modeling (converter-level), each SM is simplified into a heat source. The internal structure of the SM is neglected in order to model the relationship among different SMs and even the impact of the cabinet. The TCC effects of neighboring SMs and arm inductors are all included in the process.

A. The SM-Level Thermal Model

In the conventional 1-D Foster thermal network, junction or hotspot temperatures of components are dependent on the self-heating only. The mutual effects among different heat sources are neglected. However, any device dissipating power not only causes a temperature rise of the device itself but also all other neighboring devices. From this perspective, the SM-level thermal model considers the TCC effects, as shown in Fig. 4. Each heat source represents a power device or a capacitor. The thermal impedance is composed of self impedance and mutual impedance. The mutual impedance models the TCC effect among different components. Notably, the local ambient

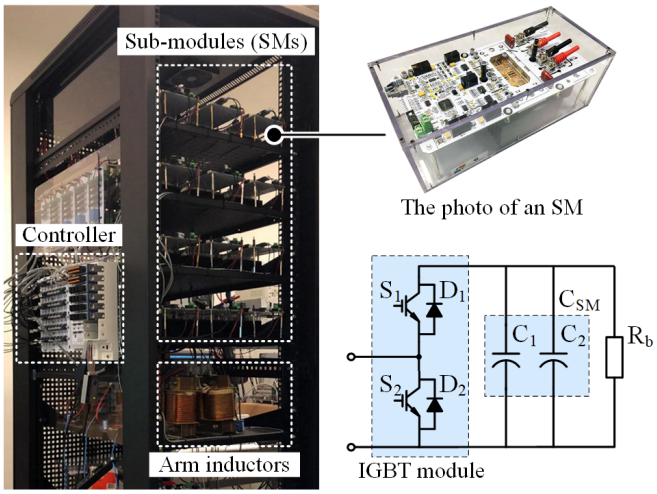

(a)

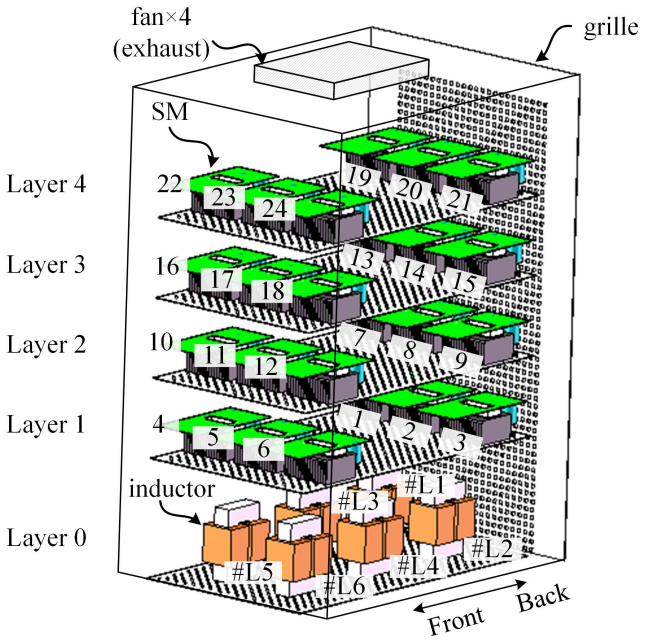

(b)

Fig. 2. A 15-kVA down-scale MMC prototype: (a) photo of the platform and the configuration of an SM and (b) 3-D layout.

temperature is defined as the ambient temperature around the SM. The thermal model can be expressed as

$$\begin{bmatrix} T_{\mathrm{j}1} \\ \vdots \\ T_{\mathrm{j}6} \end{bmatrix} = \begin{bmatrix} Z_{\mathrm{ja1},1} & \cdots & Z_{\mathrm{ja1},6} & Z_{\mathrm{ja1,R}} \\ \vdots & \ddots & \vdots & \vdots \\ Z_{\mathrm{ja6},1} & \cdots & Z_{\mathrm{ja6},6} & Z_{\mathrm{ja6,R}} \end{bmatrix} \begin{bmatrix} P_1 \\ \vdots \\ P_6 \\ P_{\mathrm{R}} \end{bmatrix} + T_{\mathrm{la}i} \tag{1}$$

where $Z_{\mathrm{ja}i,i}$ is the self-thermal impedance, $Z_{\mathrm{ja}i,i}(i \neq j)$ expresses the mutual-thermal impedance, P_1,..., P_6, P_{R} are the corresponding power losses, and $T_{\mathrm{la}i}$ is the local ambient temperature of the i-th SM.

The SM consists of multiple components, such as power

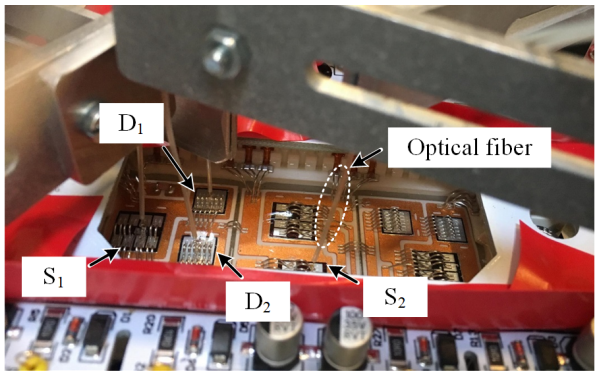

Fig. 3. Temperature measurement of four power semiconductor chips via thermo-optical fibers.

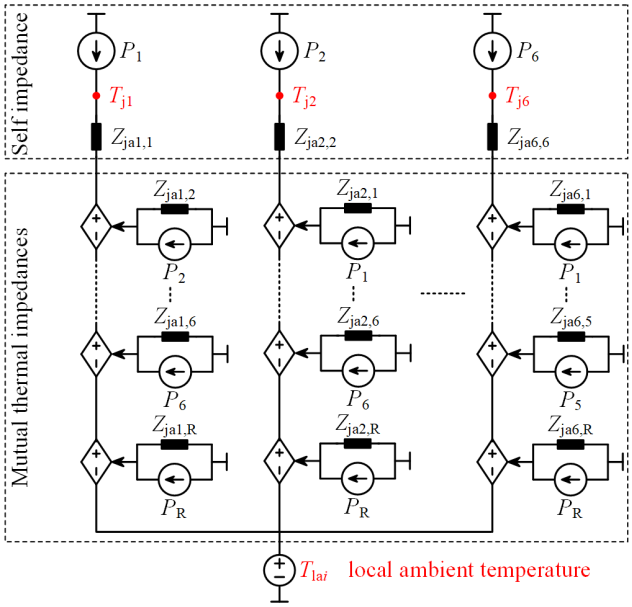

Fig. 4. The i-th SM thermal model from the junction/hotsopt temperatures of power devices or capacitors (T_{j1}–T_{j6}) to the local ambient temperature (T_{lai}).

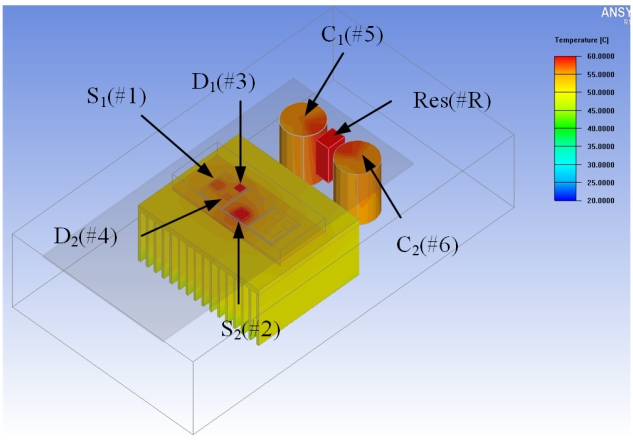

Fig. 5. The FEM model of an SM which mainly consists of four power devices, two capacitors, a bleeding resistors, PCB, and a heat sink.

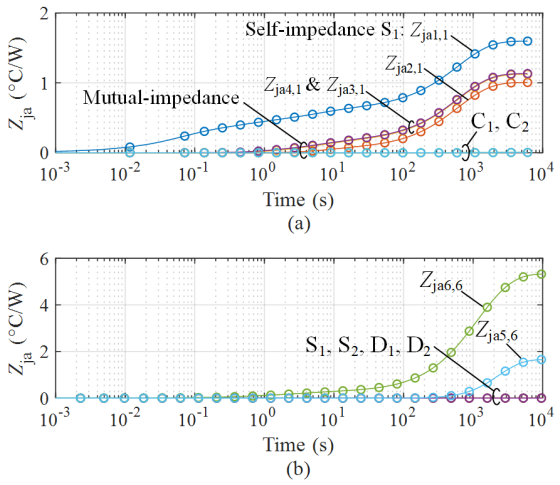

Fig. 6. FEM simulation results for the junction/hotspot-to-local ambient thermal impedances and mutual thermal impedances: (a) S_1 and (b) C_2.

modules, capacitors, bleeding resistors, Print-Circuit Board (PCB), etc. The analytical thermal model of such a complicated structure is difficult to be obtained. By contrast, the FEM simulation with ANSYS/Icepak is a feasible solution to achieve the above objective. The FEM model of an SM is shown in Fig. 5. The simulated thermal impedance of major components (i.e., power devices and capacitors) are shown in Fig. 6. The amplitude of the self thermal impedance of S_1 (denotes $Z_{ja1,1}$) is around 1.7 °C/W. Due to the shorter spatial distance, the thermal coupling effects among power devices are strong, where the mutual thermal impedance (i.e., $Z_{jai,1}$) are about half of the self thermal impedance ($Z_{ja1,1}$) By contrast, device S_1 has limited thermal impact on the capacitors. Moreover, Fig. 6(b) also shows the self thermal impedance of C_2 (i.e., $Z_{ja6,6}$=5.5 °C/W). Similarly, the contribution from capacitors to the power devices regarding the mutual thermal impedance is negligible.

B. Converter-Level Thermal Modeling

As mentioned in (1), the local ambient temperature for each SM T_{lai} is the reference to estimate the junction/hotspot temperature of devices. Its accuracy has an impact on the temperature estimation error of the devices. Conventional thermal models usually assume that the local ambient temperature is identical to the global ambient temperature, or all the devices are exposed to a homogeneous local ambient temperature. These assumptions might be reasonable when the studied case is small and has a limited number of components. However, for the MMC with hundreds or thousands of SMs, the local ambient temperature of an SM might be affected by the temperature rises of neighboring subsystems. The aforementioned assumptions are thus questionable and a converter-level model is necessary to be studied.

As shown in Fig. 7, the converter-level thermal model of the MMC simplifies the SM into a heat source without considering its internal structure. Then, by applying the thermal matrix

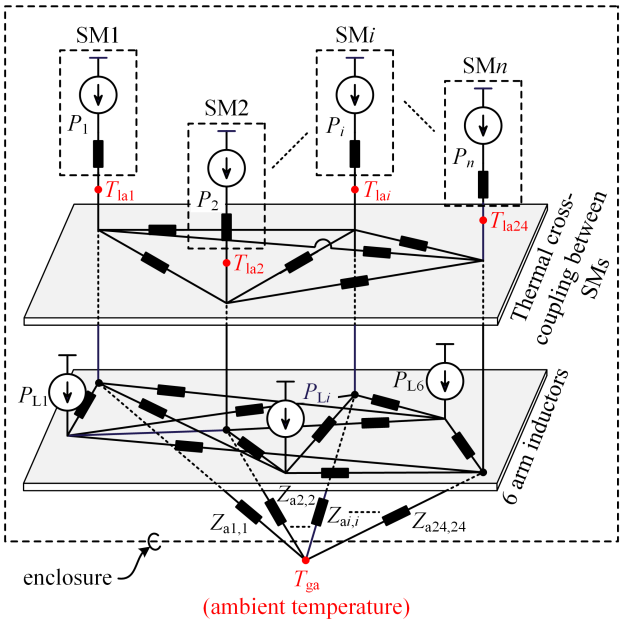

Fig. 7. The converter-level thermal model from the local ambient temperature (T_{lai}) to the global ambient temperature (T_{ga}).

method, system-level TCC effects can be evaluated by

$$\mathbf{T}_{la} = \mathbf{Z}_a \mathbf{P}_{SM/L} + T_{ga} \tag{2}$$

where $\mathbf{T}_{la}$ is the local ambient temperature vector of SMs. The local ambient-to-global ambient thermal impedance $\mathbf{Z}_a$ characterizes the TCC effects among different SMs, inductors and even the impact of the cabinet.

In this case, the local ambient-to-global ambient thermal impedances are also characterized by the FEM simulation. To reduce the computational complexity, the internal structure of SMs is simplified when simulating the complete MMC system with many SMs. The obtained transient thermal impedances are shown in Fig. 8. When SM1 on the backside of the cabinet is heated up, the rising of self-thermal impedance $Z_{a1,1}$ indicates that the local ambient temperature of SM1 increases. Meanwhile, the local ambient temperatures of the SMs (i.e., SM7, SM8, SM13, SM14, and SM19) also rise, which describe as the TCC effects among SMs. Compared to SM1, the TCC effects of SM2 on the cabinet backside are more significant, while SM3 has a similar effect to SM1 (see Figs. 8(a), (b) and (c)). Similarly, the front-side SM4 is heated up, as shown in Fig. 8(d). The TCC effects of SM4 are more noticeable compared to SM1. This is because the front cabinet is made up with airtight glass while the backside is a grille with airflow. As for SM7 shown in Fig. 8(e), its TCC effects can mainly be found among the above SMs. Besides, the effects of the inductor L1 are also depicted in Fig. 8(f). All the above phenomena reveal that the converter-level TCC effect is directional, from the bottom to the top. Moreover, different locations and different cabinet properties also affect the TCC effects among SMs. These characteristics emphasize the significance of the system layout and the cabinet.

TABLE I
SPECIFICATIONS AND PARAMETERS OF THE MMC PROTOTYPE

Parameters and symbols	Values and units
Nominal apparent power S_N	15 kVA
Nominal active power P_N	13.5 kW
DC bus voltage U_{dc}	900 V
Switching frequency f_{sw}	1.5 kHz
Leakage reactance of the transformer L_T	4 mH (0.12 p.u.)
Arm reactance L_0	4 mH (0.12 p.u.)
SM capacitance $C_{SM} = C_1 + C_2$	400 V/820 μF $\times$2
Grid line voltage at PCC U_s	380 V
Number of normal SMs per arm N	3
Number of redundant SMs per arm R	1
Bleeding resistor of each SM R_b	12 kΩ
IGBT module	1.2 kV/50 A (F4-50R12KS4)

IV. EXPERIMENTAL VERIFICATIONS

To validate the proposed thermal model, experiments are conducted based on the MMC platform under the power loading condition of 13.5 kW/6.5 kVar. Other parameters are listed in Table I. The following experimental verifications are carried out from two aspects: the SM-level and converter-level thermal modeling.

A. The SM-Level Thermal Modeling Verification

As shown in Fig. 9, the junction temperatures of the power devices and the hotspot temperatures of the capacitors are measured under the local ambient temperature of 28 °C. At the same time, estimations based on the proposed method considering TCC effects are compared with the results based on the conventional thermal model. Without considering TCC effects among different components, larger power losses are straightforward to produce higher junction/hotspot temperatures. In the experiments, the power device S_2 has the maximum power losses of 16.8 W. By contrast, the power losses of the device D_2 and the capacitors are around 1 W and less than 1 W, respectively. The highest temperature can be observed at the device S_2 and the temperature of device D_2 and capacitors are much lower. However, when the TCC effects are taken into account, corresponding simulation results are significantly different from the measurements. The junction temperature of device D_2 reaches a peak of around 60°C instead of approximately 30°C without the TCC effect, as shown in Fig. 9(d). The estimated temperature based on the proposed method agrees with the measurements within minor errors. Conclusions can be safely reached that TCC effects among different devices are significant for their thermal behavior evaluation.

B. The Converter-Level Thermal Modeling Verification

In the following, local ambient temperatures of the 24 SMs are measured as shown in Fig. 10. All the local ambient temperatures are equal to the global ambient temperature of 28°C initially (Time = 0 s). With the running of the prototype, the local ambient temperatures increase with a visible divergence. In steady-state (Time = 10000 s), the difference among these SMs is up to 17°C. The local ambient temperature of SM16 is maximum at around 58°C. Although SM6 has the lowest

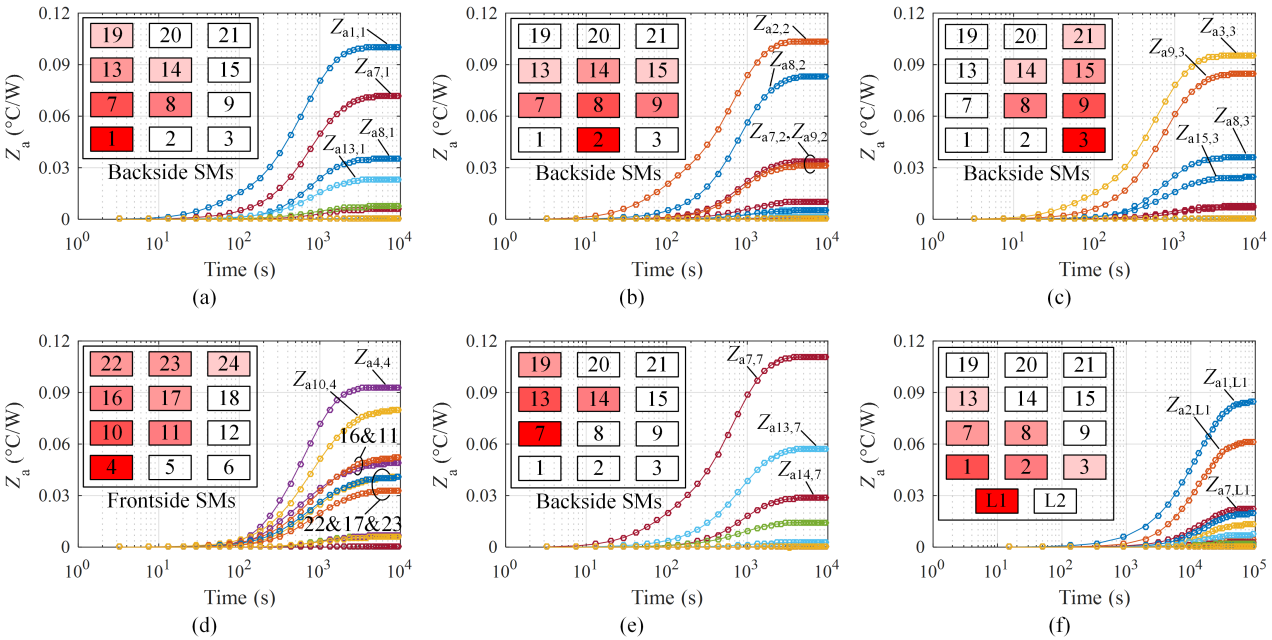

Fig. 8. The local ambient-to-global ambient thermal impedances with the heated-up of a single SM or the arm inductor respectively: (a) SM1 is heated up only, (b) SM2, (c) SM3, (d) SM4, (e) SM7 and (f) the arm inductor L1.

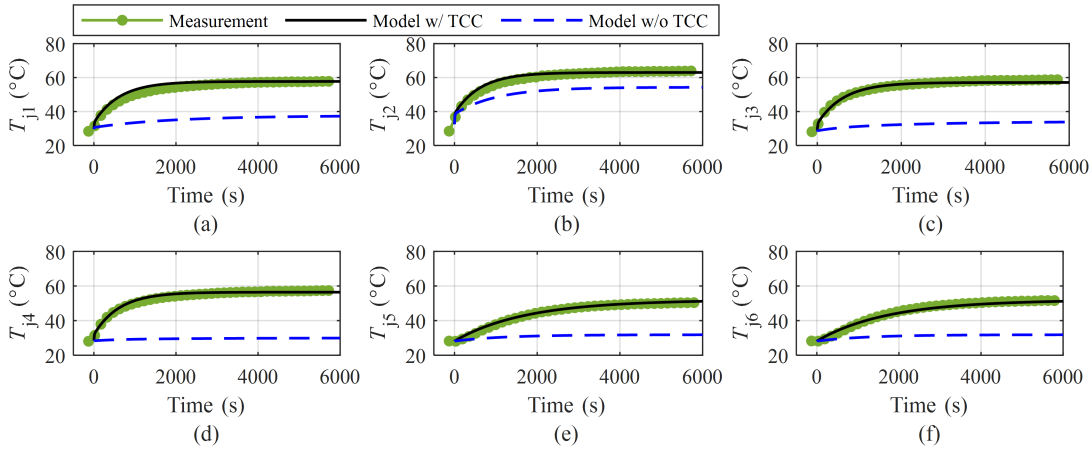

Fig. 9. Junction/hotspot temperatures of the power semiconductor devices or the capacitors: (a) S_1, (b) S_2, (c) D_1, (d) D_2, (e) C_1, and (f) C_2 (where T_{lamb}=28 °C).

local ambient temperature, T_{la6} = 41°C is still obviously higher than the global ambient temperature. Thus, if the difference between the local ambient temperature and the global ambient temperature is not considered, the device stresses will be underestimated.

Moreover, the distribution of the steady-state local ambient temperatures is shown in Fig. 11. Firstly, SMs located at a higher layer can seen a higher local ambient temperature. For example, SMs in the 4th-layer has higher local ambient temperatures than that in the 1st-layer. Afterward, the first three SMs of each layer are assembled on the back-side of the cabinet, while the other three SMs are located at the front side (see Fig. 2). The front-side SMs have higher local ambient temperatures compared to the back-side SMs in most cases. This is due to different cabinet material properties of the back side (metallic grille with airflow) and the front side (air tight glass). These experimental results reveal the significance of the layout and properties of the cabinet.

Furthermore, Fig. 12 compares the measured local ambient temperatures to the estimated values. Although small differences can be observed during the transient, the estimated results at steady-state are in good agreement with each other. Thus, with consideration of the TCC effects among different SMs, the proposed converter-level thermal modeling can provide a more accurate thermal estimation.

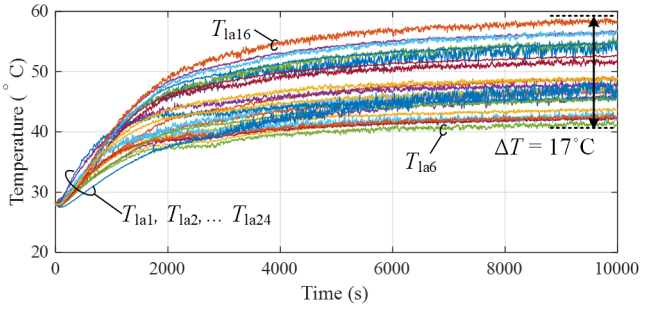

Fig. 10. Measured local ambient temperatures of 24 SMs in the MMC platform, where the global ambient temperature is 28°C.

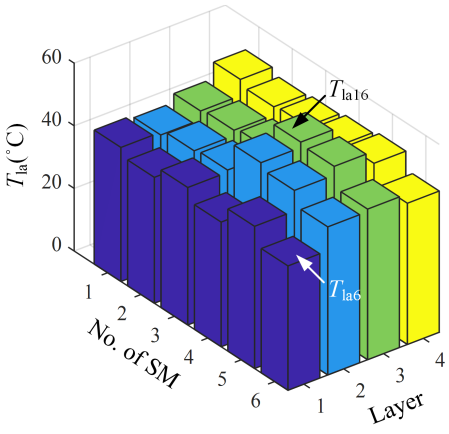

Fig. 11. Measured local ambient temperatures of 24 SMs in the MMC platform, where active and reactive powers are 13.5 kW and 6.5 kVar, and global ambient temperature is 28°C.

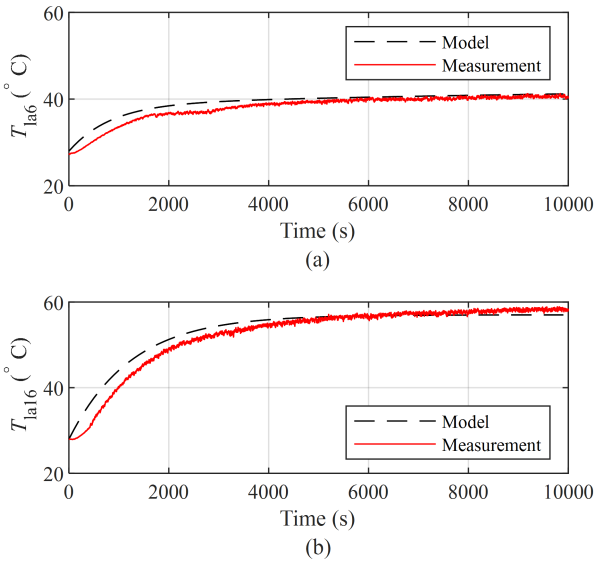

Fig. 12. Comparison of the measured local ambient temperatures and the estimated results of two SMs: (a) SM6 and (b) SM16.

V. Conclusion

This paper proposes a systematical thermal model of the MMC via two hierarchical decompositions. The first SM-level thermal model considers the TCC effects among different components. Subsequently, the second system-level thermal model provides a more accurate temperature reference for the SM-level thermal estimation. The in-situ measurements show that the TCC effects significantly affect thermal estimation. An error of 45% is observed based on the model without considering TCC effects. Moreover, the local ambient temperatures of SMs are significantly affected by different assembling locations and the properties of the cabinet. The local ambient temperatures of these SMs are divergent with a difference up to 17°C. The minimum local ambient temperature in the prototype is more than 10°C higher than the global ambient temperature. These results emphasize that the physical layouts from components, SMs, to the system are of great significance for the thermal estimation.

References

[1] CIGRE, *Technical brochure 619, HVDC connection of offshore wind power plants*. CIGRE Working Group B4.55, 2015.

[2] M. Hagiwara, K. Nishimura, and H. Akagi, "A medium-voltage motor drive with a modular multilevel PWM inverter," *IEEE Trans. Power Electron.*, vol. 25, no. 7, pp. 1786–1799, Jul. 2010.

[3] A. Antonopoulos, L. Ängquist, S. Norrga, K. Ilves, L. Harnefors, and H. P. Nee, "Modular multilevel converter AC motor drives with constant torque from zero to nominal speed," *IEEE Trans. Ind. Appl.*, vol. 50, no. 3, pp. 1982–1993, May/Jun. 2014.

[4] H. Wang, G. Tang, Z. He, and J. Yang, "Efficient grounding for modular multilevel HVDC converters (MMC) on the AC side," *IEEE Trans. Power Deliv.*, vol. 29, no. 3, pp. 1262–1272, Jun. 2014.

[5] J. Glasdam, J. Hjerrild, L. H. Kocewiak, and C. L. Bak, "Review on multi-level voltage source converter based HVDC technologies for grid connection of large offshore wind farms," in *Proc. IEEE Int. Conf. Power Syst. Technol. POWERCON*, 2012, pp. 1–6.

[6] H. Wang, M. Liserre, F. Blaabjerg, P. de Place Rimmen, J. B. Jacobsen, T. Kvisgaard, and J. Landkildehus, "Transitioning to physics-of-failure as a reliability driver in power electronics," *IEEE Trans. Emerg. Sel. Topics Power Electron.*, vol. 2, no. 1, pp. 97–114, Mar. 2014.

[7] H. Liu, K. Ma, Z. Qin, P. C. Loh, and F. Blaabjerg, "Lifetime estimation of MMC for offshore wind power HVDC application," *IEEE J. Emerg. Sel. Topics Power Electron.*, vol. 4, no. 2, pp. 504–511, Sep. 2016.

[8] F. Hahn, M. Andresen, G. Buticchi, and M. Liserre, "Thermal analysis and balancing for modular multilevel converters in HVDC applications," *IEEE Trans. Power Electron.*, vol. 33, no. 3, pp. 1985–1996, Mar. 2018.

[9] W. Li, H. Yang, J. Sheng, C. Li, M. Chen, X. He, and X. Gu, "Thermal optimization of modular multilevel converters with surplus sub-module active-bypass plus neutral-point-shift scheme under unbalanced grid," *IEEE J. Emerg. Sel. Top. Power Electron.*, vol. PP, no. c, pp. 1–1, Early acess, 2019.

[10] J. Goncalves, D. J. Rogers, and J. Liang, "Submodule temperature regulation and balancing in modular multilevel converters," *IEEE Trans. Ind. Electron.*, vol. 65, no. 9, pp. 7085–7094, Sept. 2018.

[11] Y. Dong, H. Yang, W. Li, and X. He, "Neutral-point-shift-based active thermal control for a modular multilevel converter under a single-phase-to-ground fault," *IEEE Trans. Ind. Electron.*, vol. 66, no. 3, pp. 2474–2484, 2019.

[12] S. Thomas, "Infineon AN2008-03: Thermal equivalent circuit models," Tech. Rep., 2008.

[13] A. S. Bahman, K. Ma, P. Ghimire, F. Iannuzzo, and F. Blaabjerg, "A 3-D-lumped thermal network model for long-term load profiles analysis in high-power IGBT modules," *IEEE J. Emerg. Sel. Top. Power Electron.*, vol. 4, no. 3, pp. 1050–1063, Sept. 2016.

[14] Y. Shen, A. Chub, H. Wang, D. Vinnikov, E. Liivik, and F. Blaabjerg, "Wear-out failure analysis of an impedance-source PV microinverter based on system-level electrothermal modeling," *IEEE Trans. Ind. Electron.*, vol. 66, no. 5, pp. 3914–3927, May 2019.